

Communication

# Charged Kaon Femtoscopy with Lévy Sources in $\sqrt{s_{NN}} = 200$ GeV Au+Au Collisions at PHENIX

László Kovács on behalf of the PHENIX Collaboration

Department of Atomic Physics, Faculty of Science, Eötvös Loránd University, Pázmány Péter Sétány 1/A, H-1111 Budapest, Hungary; kovacs.laszlo9201@gmail.com

**Abstract:** The PHENIX experiment measured two-particle Bose–Einstein quantum-statistical correlations of charged kaons in Au+Au collisions at  $\sqrt{s_{NN}} = 200$  GeV. The correlation functions are parametrized assuming that the source emitting the particles has a Lévy shape, characterized by the Lévy exponent  $\alpha$  and the Lévy scale  $R$ . By introducing the intercept parameter  $\lambda$ , we account for the core–halo fraction. The parameters are investigated as a function of transverse mass. The comparison of the parameters measured for kaon–kaon with those measured from pion–pion correlation may clarify the connection of Lévy parameters to physical processes .

**Keywords:** heavy ions; quark–gluon plasma; femtoscopy; Lévy HBT

## 1. Introduction

To study the space-time structure of the quark–gluon plasma, the most commonly used method is femtoscopy. It is a sub-field of high-energy particles and nuclear physics, and it allows us to explore the properties of the matter created in particle collisions on the femtometer scale. Femtoscopy typically investigates correlations of particle pairs. However, it is worth mentioning that prior to the development of femtoscopy, a similar physical phenomenon was discovered and utilized in the field of radio astronomy. R. Hanbury Brown and R. Q. Twiss measured the angular size of stars by analyzing intensity correlations, which became known as the Hanbury Brown and Twiss effect (HBT) [1]. Roy Glauber’s work that laid the foundations of quantum optics [2–4] greatly increased our understanding of this effect. G. Goldhaber and his collaborators observed intensity correlations among same-charged pions while searching for  $\rho$  mesons in high-energy collisions. These correlations were explained by G. Goldhaber, S. Goldhaber, W-Y. Lee, and A. Pais (GGLP), based on the Bose–Einstein symmetrization of the wave-function of identical pion pairs [5]. This is the reason why these correlations are often called Bose–Einstein correlations. Due to the relationship between the two-particle Bose–Einstein correlation function and the phase-space density of the particle-emitting source, by measuring the correlation function we can obtain information about the source function.

Let us note that while there are conceptual similarities between the HBT effect in radio astronomy and the correlations studied in femtoscopy, there are also fundamental differences. In femtoscopy, we can extract information about the space-time structure of the particle source, often represented by femtosopic radii. On the other hand, the HBT effect in radio astronomy provides insights into the spectral-angular structure of the source radiation.

The fundamentals of modern correlation femtoscopy were established by Kopylov and Podgoretsky [6,7]. They successfully overcame the drawback of the GGLP technique by utilizing the momentum differences of the particle pairs instead of the opening angles.

Based on the central limit theorem, it is a good approach to assume a Gaussian shape for the phase-space density of the particle-emitting source. However, we can go further and take a more general approach. Anomalous diffusion indicates the appearance of Lévy-stable distributions for the source [8,9]. In Ref. [10], it was found that Lévy-stable



**Citation:** Kovács, L., on behalf of the PHENIX Collaboration. Charged Kaon Femtoscopy with Lévy Sources in  $\sqrt{s_{NN}} = 200$  GeV Au+Au Collisions at PHENIX. *Universe* **2023**, *9*, 336. <https://doi.org/10.3390/universe9070336>

Academic Editor: Jun Xu

Received: 30 May 2023

Revised: 8 July 2023

Accepted: 11 July 2023

Published: 17 July 2023



**Copyright:** © 2023 by the authors. Licensee MDPI, Basel, Switzerland. This article is an open access article distributed under the terms and conditions of the Creative Commons Attribution (CC BY) license (<https://creativecommons.org/licenses/by/4.0/>).

source distributions in  $\sqrt{s_{NN}} = 200$  GeV Au+Au collisions give a high-quality, statistically acceptable description of the measured correlation functions in the case of pions. In the present paper, we will investigate kaon–kaon correlation functions assuming a Lévy shaped source. By comparing the obtained results with the pion data, more insights can be gained regarding the Lévy parameters.

The dataset used in this analysis is Au+Au collisions at  $\sqrt{s_{NN}} = 200$  GeV recorded by the PHENIX (Pioneering High Energy Nuclear Interaction eXperiment) detector. It is one of the four experiments that have taken data at the relativistic heavy ion collider (RHIC) in Brookhaven National Laboratory. Its primary mission was to search for a new state of matter called the quark–gluon plasma and to study various different particle types produced in heavy ion collisions, such as photons, electrons, muons, and charged hadrons. A beam view layout of the PHENIX detector can be seen in Figure 1. The detectors can be divided into four main subgroups:

1. Global detectors characterize the nature of heavy ion collision events, i.e., zero degree calorimeters (ZDC) and beam-beam counters (BBC);
2. Mid-rapidity detectors form the “central arm spectrometer”, which consists of three sets of pad chambers (PC), drift chambers (DC), electromagnetic calorimeters (Em-Cal), and time-of-flight detectors (ToF), are used for energy, momentum, and mass measurements;
3. Two muon spectrometers at forward rapidity;
4. A triggering and computing system to select and archive events of potential physics interest.

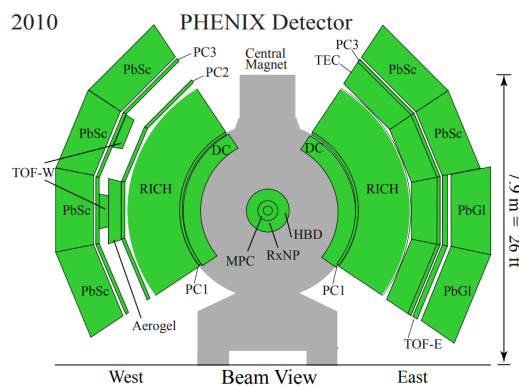


Figure 1. View of the PHENIX central arm spectrometer detector setup in the 2010 data-taking period.

## 2. Femtoscopy and Lévy Sources

As we mentioned in the previous section, there is a connection between the Bose–Einstein correlation function and the phase-space density of the particle-emitting source. Let us discuss this relationship in more detail. The one- and two-particle momentum distributions can be expressed as [11]

$$N_1(p) = \int d^4r S(r, p) |\psi_p(r)|^2, \tag{1}$$

$$N_2(p_1, p_2) = \int d^4r_1 d^4r_2 S(r_1, p_1) S(r_2, p_2) |\psi_{p_1, p_2}^{(2)}(r_1, r_2)|^2, \tag{2}$$

where  $S(r, p)$  is the source function, which describes the probability density of particle creation at space-time point  $r$  with four-momentum  $p$ ;  $\psi_p(r)$  denotes the single-particle wave function; and  $\psi_{p_1, p_2}^{(2)}$  is the two-particle wave function, which must be symmetric in the spatial variables  $r_1$  and  $r_2$  for bosons. Bose–Einstein correlations arise from this sym-

metrization effect. Using Equations (1) and (2), we can express the two-particle correlation function as [12,13]

$$C_2(p_1, p_2) = \frac{N_2(p_1, p_2)}{N_1(p_1)N_1(p_2)}. \tag{3}$$

Let us introduce the average momentum  $K = 0.5(p_1 + p_2)$  and relative momentum  $q = p_1 - p_2$  as new variables. If  $p_1 \approx p_2 \approx K$  and the final state interactions are neglected, the two-particle correlation function can be written as

$$C_2^{(0)}(q, K) \approx 1 + \frac{|\tilde{S}(q, K)|^2}{|\tilde{S}(0, K)|^2}, \tag{4}$$

where the superscript (0) denotes the neglect of final state interactions and  $\tilde{S}(q, K)$  is the Fourier transform of the source with

$$\tilde{S}(q, K) = \int S(x, K) e^{iqx} d^4x. \tag{5}$$

The significance of Equation (4) lies in the fact that by measuring the Bose–Einstein correlation function, we can obtain information about the spatial shape of the source function.

The correlation function depends on the four-momentum difference and the average four-momentum. Since the Lorentz product of  $q$  and  $K$  is zero in the case of identical particles, the correlation function depends only on the spatial  $\mathbf{q}$  instead of the four dimensional  $q$  vector:

$$qK = q_0K_0 - \mathbf{q}\mathbf{K} = 0 \Rightarrow q_0 = \frac{\mathbf{q}\mathbf{K}}{K_0}. \tag{6}$$

In Ref. [7], Kopylov and Podgoretsky showcased the three-dimensional character of the momentum correlation effect due to the particles detected on-mass-shell.

For our correlation function measurements, we use the co-moving system (LCMS) frame, where it was found in earlier measurements [14] that the correlation function is nearly spherically symmetric. Due to the relatively low number of produced kaons and this symmetrical characteristic, we have chosen to perform a one-dimensional (1D) analysis instead of a three-dimensional (3D) one. Based on Ref. [10], we used  $Q = |q_{\text{LCMS}}|$  as the 1D variable of the correlation function.

We assumed that the source emitting the particles has a Lévy shape. The symmetric Lévy-stable distribution is defined as

$$\mathcal{L}(\mathbf{r}; R, \alpha) = \frac{1}{(2\pi)^3} \int d^3\boldsymbol{\varphi} e^{i\boldsymbol{\varphi}\mathbf{r}} e^{-\frac{1}{2}|\boldsymbol{\varphi}R|^\alpha}, \tag{7}$$

where  $R$  is the Lévy scale parameter,  $\alpha$  is the Lévy exponent, and  $\boldsymbol{\varphi}$  is a three-dimensional integration variable. The  $\alpha$  parameter describes the shape of the distribution, in the case of a Gaussian distribution  $\alpha = 2$ , while for a Cauchy distribution, the value of  $\alpha$  is 1.

In case of such Lévy-stable source functions, the raw (i.e., final-state interaction neglected) correlation function in the observable  $Q$ -range will be [8]

$$C_2^{(0)}(Q; \lambda, R, \alpha) = 1 + \lambda e^{-|QR|^\alpha}, \tag{8}$$

where the intercept parameter  $\lambda$  is introduced as the extrapolated  $C_2^{(0)}(Q = 0)$  value.

According to the core–halo model [15,16], the source can be divided into two parts: the core, which contains the promptly produced particles, and the halo, which is composed

of the products of resonance decays. The ratio of these two parts can be characterized by the correlation strength parameter:

$$\lambda = \left( \frac{N_{\text{core}}}{N_{\text{core}} + N_{\text{halo}}} \right)^2, \tag{9}$$

where  $N_{\text{core}}$  refers to the number of particles produced in the core, while  $N_{\text{halo}}$  denotes the number of particles produced in the halo. Considering that the particles from the halo contribute to the correlation function as an unresolvably narrow peak around  $Q = 0$ , we indeed see that this  $\lambda$  value will be the extrapolated  $C_2^{(0)}(Q = 0)$  value.

For charged particles, the most significant final state interaction is the Coulomb interaction. To take care of this effect, we used the Sinyukov–Bowler method [17,18]. Taking an additional possible linear background shape into account, our final assumption for the functional form of the correlation function is

$$C_2(Q; \lambda, R, \alpha) = \left[ 1 - \lambda + K(q_{\text{inv}}; \alpha, R) \cdot \lambda \cdot \left( 1 + e^{-|QR|^\alpha} \right) \right] \cdot N \cdot (1 + \epsilon Q), \tag{10}$$

where  $K$  is the Coulomb correction,  $N$  is the normalization parameter, and  $\epsilon$  represents a small background long-range correlation effect. Let us note that the Coulomb correction is a function of  $q_{\text{inv}}$ , which is the Lorentz invariant four-momentum difference<sup>1</sup>, while the correlation function has a different variable, denoted by  $Q$ . We calculated the Coulomb correction  $K$  with the variable  $Q$  and analyzed the error coming from this approximation, which was handled as a source of systematic uncertainty the same way as in Ref. [10]. The correction is quite small compared to other sources, so it does not mean a large additional term to the systematics, and this way we have more comparable results to the pions.

### 3. Motivation

In Ref. [10], the significance of the appearance of the Lévy distribution in the case of pion–pion correlations was investigated. In order to dive into the exploration of the Lévy-shape, we aimed to analyze kaon correlations.

The Lévy source parameters for kaon–kaon two particle correlations have never been measured in PHENIX before.

Anomalous diffusion could be a reason for a Lévy distribution [19]. In such a scenario, the Lévy index for the different particles is different, i.e.,  $\alpha_{\text{Lévy}}^\pi \neq \alpha_{\text{Lévy}}^K$ . The smaller the cross section is, the longer the mean free path, thus the longer the power-law like “tail” of the source distribution. Kaons have a smaller cross section than pions, so we would expect that  $\alpha_{\text{Lévy}}^\pi > \alpha_{\text{Lévy}}^K$ . If this explanation fails to match the reality, other alternatives should be investigated.

The Lévy width (or, equivalently, scale parameter)  $R$  has an unclear interpretation. It exhibits similar behavior as the Gaussian source radii, but its precise relation to the geometrical source size is not clear. By measuring this parameter for kaons, we can get closer to clarifying its precise physical interpretation.

### 4. Measurement Details

In this measurement, we analyzed Au+Au collisions at  $\sqrt{s_{\text{NN}}} = 200$  GeV. The dataset consists of about 7.3 billion (minimum bias triggered) events. As the number of produced kaons is relatively low, all minimum bias events (of any centrality) were taken together. We cut out those events whose distance from the nominal collision point was greater than 30 cm along the beam axis.

We also need to take into account the detector inefficiencies and the particularities of the track reconstruction algorithm, which sometimes splits one track into two. On the other hand, when two different tracks are too close to each other, it is possible that they will be detected as a single track. To remove these possible effects, we applied cuts in the

$\Delta\phi$  and  $\Delta z$  variables, where  $\Delta\phi$  and  $\Delta z$  stand for the azimuthal angle and longitudinal position difference of track pairs, respectively (as measured in the drift chamber, the main tracking detector).

For particle identification (PID), we calculated the square of the particle mass:

$$m^2 = \frac{\mathbf{p}^2}{c^2} \left[ \left( \frac{ct}{L} \right)^2 - 1 \right], \tag{11}$$

where  $t$  is the time of flight (measured either in the PbSc or the ToF East/West detectors),  $L$  is the path length, and  $\mathbf{p}$  is the momentum. The distributions of  $m^2$  were fitted mostly using single Gaussians; in cases of merging peaks, a double Gaussian was applied. To identify kaons, we applied a  $2.5\sigma_p$  cut around the nominal kaon  $m^2$  peak position and a  $2.5\sigma_p$  veto cut around the pion and proton  $m^2$  peaks. An example scatter plot of the charge times momentum vs.  $m^2$  before and after the cuts can be seen in Figure 2a,b, respectively.

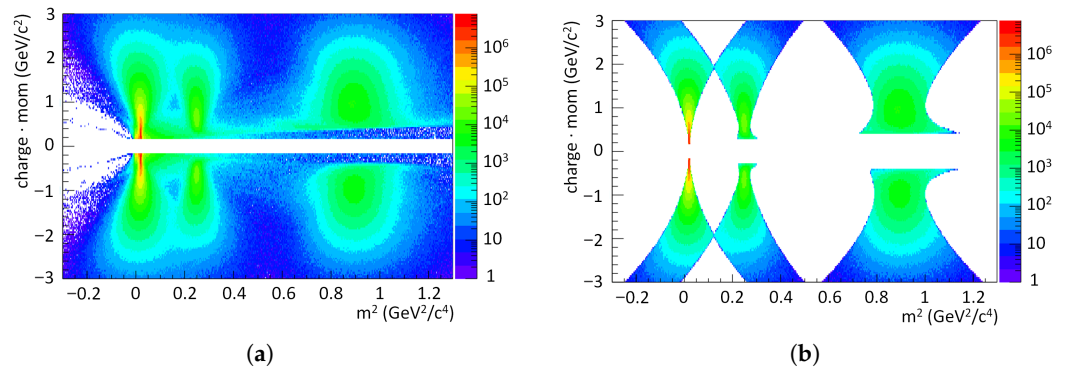


**Figure 2.** Example plots for PID. (a) Scatter plot of the charge times momentum vs.  $m^2$  in TOF West with no cut. (b) Scatter plot of the charge times momentum vs.  $m^2$  in TOF West after the applied cuts.

Since the correlation function’s dependence on  $K$  is smoother than its dependence on  $Q$ , it is reasonable to create several  $K$  bins, and in each bin, the  $Q$  dependence can be investigated. At midrapidity, the transverse mass  $m_T$  can be used instead of  $K$ :

$$m_T = \sqrt{m^2 + (K_T/c)^2}, \tag{12}$$

where  $m$  is the mass of the particle and

$$K_T = \sqrt{K_x^2 + K_y^2} \tag{13}$$

is the average transverse momentum. In this analysis, 7  $m_T$  bins were created. In each bin, we analyzed the dependence of the correlation function on  $Q$ .

To measure the correlation functions, “actual” (foreground) and “background” distributions of the kaon pairs were created. To construct the actual pair distribution, the momentum differences were calculated of the same-charged particles from the same event and filled into a histogram. Since there are other effects (stemming from acceptance, single-particle distributions, efficiency, etc.) in the actual pair distribution that are not related to the HBT effect, we have to cancel them out with a properly constructed background distribution that contains pairs from different events, where there can be no HBT effect. To create the background pair distribution, we employed the same mixed event method as described in Ref. [10]. The first step is to construct a pool that contains several events. This pool needs to be at least as large as the number of produced kaons in the event with the highest multiplicity. In order to ensure that we meet this condition, a pool with 50 events was used. Every time we process an event to construct the actual pair distribution, we construct a mixed event for the background distribution as well. Since we do not want to introduce any

correlations and we would like to avoid the presence of the quantum-statistical correlation between the particles in the background, we have to select the particles as follows. First of all, to ensure that the background event exhibits the same kinematics and acceptance effects, we have to construct the background event from events of similar centrality and with a similar  $z$  coordinate of the collision vertex. To accomplish this, we used 5% wide centrality and 2 cm wide  $z$ -vertex bins. Secondly, it is essential that the selected particles for the background pair distribution originate from different events. After the particle selection from mixed events we calculate the momentum differences of these particles.

The two-particle correlation function can be calculated from the ratio of the normalized actual and background pair distributions:

$$C_2(m_T, Q) = \frac{A(m_T, Q)}{B(m_T, Q)} \cdot \frac{\int_{Q_{\min}}^{Q_{\max}} B(m_T, Q)}{\int_{Q_{\min}}^{Q_{\max}} A(m_T, Q)}, \quad (14)$$

where  $A$  is the actual,  $B$  is the background pair distribution, and the integral is performed over a range  $(Q_{\min} - Q_{\max})$ , where the correlation function does not exhibit quantum statistical features.

We fitted the measured correlation functions with the Coulomb-corrected Lévy-type correlation function and the linear background. Of all the final state interactions, the Coulomb effect has the greatest impact as it causes same-charged pairs to repel each other. As shown in Figure 3, the function drops off sharply at small  $Q$  due to the Coulomb effect.

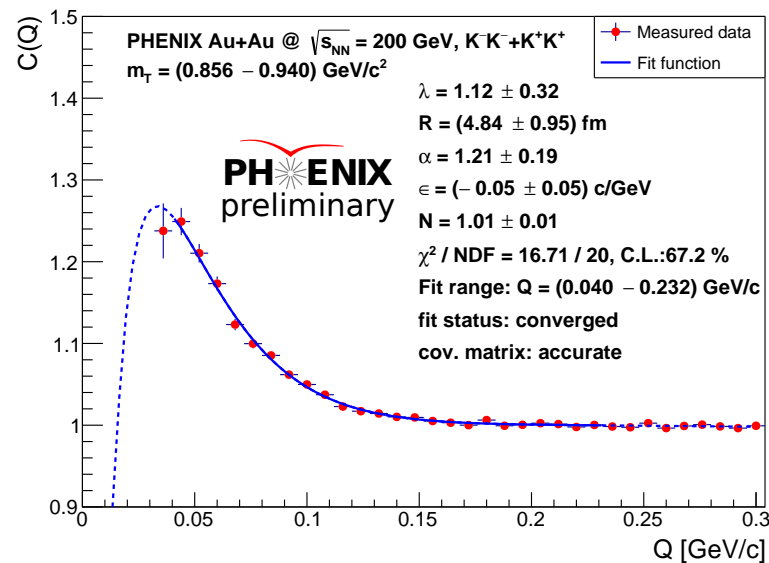


**Figure 3.** An example fit with the Coulomb-corrected correlation function based on a Lévy source for kaon pairs with transverse mass ranging from 0.856 GeV/ $c^2$  to 0.940 GeV/ $c^2$ .

To deal with the Coulomb correction, we applied the same method that was used in Ref. [10] for pions; we did this to obtain comparable results. First, we needed to numerically solve the Coulomb correction; then, the results were loaded into a binary look up table as described in Refs. [20,21]. This numerical table contains the values discretely, so interpolation was needed, which can cause numerical fluctuations. These fluctuations can be handled with a proper iterative fitting procedure. The first round fit was performed with a functional form of the correlation function incorporating the Coulomb correction, which yields a set of parameters  $\lambda_0$ ,  $R_0$ , and  $\alpha_0$ . Based on Equation (10), the second round fit was with

$$C_2^{(0)}(Q; \lambda, R, \alpha) \frac{C_2(Q; \lambda_n, R_n, \alpha_n)}{C_2^{(0)}(Q; \lambda_n, R_n, \alpha_n)} \cdot N \cdot (1 + \epsilon Q), \quad (15)$$

where the fitted parameters are denoted as  $\lambda, R, \alpha, N$ , and  $\epsilon$ . In the second round, the values of  $\lambda_n, R_n$ , and  $\alpha_n$  were equal to the corresponding values from the first fit. The correlation function without the Coulomb correction is denoted by  $C_2^{(0)}(Q; \lambda, R, \alpha)$ , while  $C_2(Q; \lambda, R, \alpha)$  refers to the Coulomb-corrected one. We continued this iterative procedure until the parameters of the previous fit  $(\lambda_n, R_n, \alpha_n)$  and the new ones from the latest fit  $(\lambda_{n+1}, R_{n+1}, \alpha_{n+1})$  differed less than 2%. Let us note that usually  $N \approx 1$  and  $\epsilon \approx 0$ , and these parameters converge faster than  $\lambda, R$  and  $\alpha$ , so only the latter parameters are used in the test of the convergence criteria.

To determine the systematic uncertainties of the parameters, alternative measurement settings were applied. These considered settings can be seen in Table 1. In case of the PID cut, the default setting was  $2.5\sigma_p$ , while the lower one was  $2.0\sigma_p$  and the upper one was  $3.0\sigma_p$ . As for the PC3 matching cut, there was no cut in the default setting, but an alternative cut of  $2.0\sigma_m$  was applied, where  $\sigma_m$  is the standard deviation of the difference of the projected track position and the closest hit position in the detector, in both the  $\phi$  and  $z$  directions. Regarding the EMCal/ToF track matching cut, the default setting was  $1.5\sigma_m$ , while the lower one was  $1.0\sigma_m$  and the upper one was  $3.5\sigma_m$ . Pair cuts were applied in the  $\Delta\phi - \Delta z$  plane by cutting off a two-dimensional region, as described in Ref. [10]. The fit range ( $Q_{\min} - Q_{\max}$ ) was also varied. We modified the default setting with  $\pm 8 \text{ MeV}/c$ . As we mentioned earlier in this paper, the Coulomb correction is a function of  $q_{\text{inv}}$ , while the correlation function has a different variable, denoted by  $Q$ . We calculated the Coulomb correction with the variable  $Q$  and treated this approximation as a systematic uncertainty. The parameters were recalculated by individually changing each of the measurement settings; then, we calculated the relative difference of the values of the parameters obtained from the alternative settings and from the default settings. After calculating the relative differences for all the settings, we obtained the final systematics by taking into account the statistical uncertainties of the data points. A similar argument can be found in Ref. [22].

**Table 1.** The varied settings in order to determine the systematic uncertainties of the results.

Setting Name	Settings
PID cut	3 cut settings
PC3 matching cut	1 cut setting
EMCal/ToF matching cut	3 cut settings
DC pair cut	3 cut settings
ToF East pair cut	3 cut settings
ToF West pair cut	3 cut settings
EMCal pair cut	3 cut settings
Fit range ( $Q_{\max}$ )	3 ranges
Fit range ( $Q_{\min}$ )	3 ranges
Coulomb correction variable	2 versions

The method we used is described below. The variance of the difference of two variables is

$$\sigma^2(A_{\text{def}} - A_{\text{alt}}) = \sigma^2(A_{\text{def}}) + \sigma^2(A_{\text{alt}}) - 2\text{cov}(A_{\text{def}}, A_{\text{alt}}), \tag{16}$$

where  $A_{\text{def}}$  represents the parameter value obtained from the default cut, while  $A_{\text{alt}}$ , the parameter value, is obtained from the alternative cut;  $\text{cov}(A_{\text{def}}, A_{\text{alt}}) = \rho\sigma(A_{\text{def}})\sigma(A_{\text{alt}})$  is the covariance matrix; and  $\rho$  is the correlation coefficient. The total uncertainties are composed of the systematic and the statistical uncertainties:

$$\sigma_{\text{tot}}^2 = \sigma_{\text{stat}}^2 + \sigma_{\text{syst}}^2 \qquad \text{so} \qquad \sigma_{\text{syst}}^2 = \sigma_{\text{tot}}^2 - \sigma_{\text{stat}}^2. \tag{17}$$

We require that the total uncertainty cover 1 standard deviation ( $1\sigma$ ), i.e.,  $\sigma_{\text{tot}} = |A_{\text{def}} - A_{\text{alt}}|$ . Thus,

$$\sigma_{\text{syst}}^2 = (A_{\text{def}} - A_{\text{alt}})^2 - \sigma_{\text{stat}}^2(A_{\text{def}}) - \sigma_{\text{stat}}^2(A_{\text{alt}}) + 2\rho\sigma_{\text{stat}}(A_{\text{def}})\sigma_{\text{stat}}(A_{\text{alt}}). \quad (18)$$

The advantage of using Equation (18) is that it allows us to consider the impact of the statistical uncertainties. In this analysis, we assumed that  $A_{\text{def}}$  is completely correlated with  $A_{\text{alt}}$ , thus  $\rho = 1$ . The final systematic uncertainties were obtained by taking the squared sum of the calculated  $\sigma_{\text{syst}}$  values for each alternative setting.

### 5. Results

In this section, we present our main results: a comparison of the transverse mass dependence of the Lévy parameters in the case of kaon–kaon and pion–pion correlations.

One of the main reasons why analyzing the kaon–kaon Lévy distribution is interesting is because it could shed light on the physical interpretation of the Lévy exponent. The Lévy exponent  $\alpha$  is shown in Figure 4. Within statistical uncertainties, we can draw the conclusion that the value of the parameter is between 1 and 2; however, the systematic uncertainties are quite large. As it is described in Ref. [19], a higher  $\alpha$  value is expected for pions than for kaons based on the anomalous diffusion; however, we cannot observe this trend here, which indicates that beside anomalous diffusion of hadrons, there may be other physical processes causing the appearance of Lévy distributions, such as the resonances, as was concluded in Ref. [23]. The violation of the  $m_T$ -scaling of the two-pion and two-kaon correlations suggested by hydrodynamic models was explained by a rescattering phase in Ref. [24], which was not taken into account in the pure hydrodynamic models. A slight increase in the  $\alpha$  values of the kaon measurements can be observed, although the large uncertainties do not allow us to draw any strong conclusions.

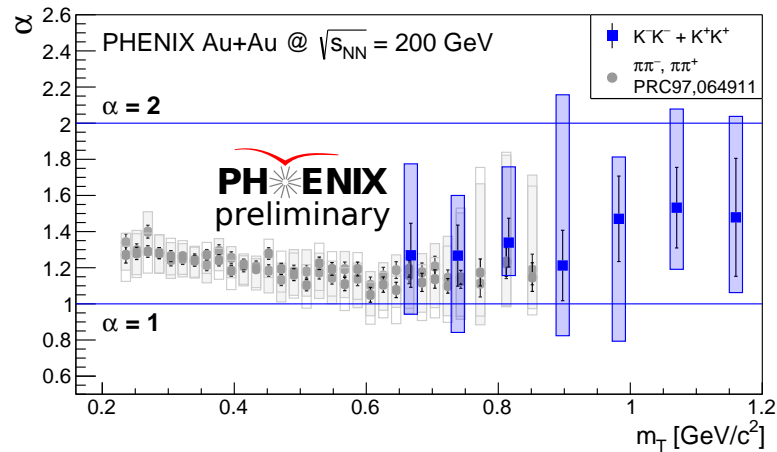


**Figure 4.** Values of the  $\alpha$  parameter in the case of pions and kaons. Boxes indicate the systematic uncertainties, while error bars are used to represent the statistical ones.

The transverse mass dependence of the intercept parameter  $\lambda$  is shown in Figure 5. Compared to the pion data, it is not inconsistent with the given large uncertainties, having approximately matching values at around  $m_T = 0.7 \text{ GeV}/c^2$ , although their trends appear to be different. No significant  $m_T$  dependence was observed for this parameter, and it is fairly constant; however, we have to note that a slight decreasing trend is visible. This parameter characterizes the strength of the correlation as it was introduced as the extrapolated  $C_2^{(0)}(Q = 0)$  value. Since there is no correlation between particles of different species, a possible worsening of PID efficiency may cause a decrease in the value of this parameter as our dataset may contain particles other than kaons.

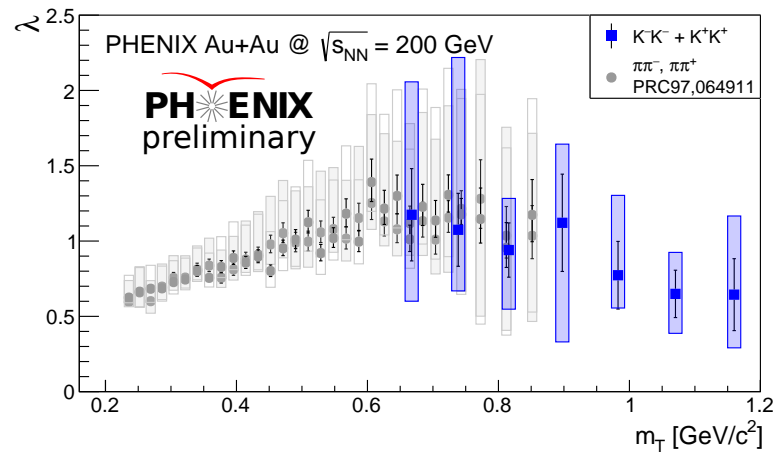


**Figure 5.** Values of the  $\lambda$  parameter in the case of pions and kaons. Boxes indicate the systematic uncertainties, while error bars are used to represent the statistical ones.

The transverse mass dependence of the Lévy scale parameter  $R$  is shown in Figure 6. The  $m_T$  scaling of HBT radii across particle species has been predicted in Ref. [25]. From theoretical works, e.g., Refs. [8,26], we know that  $R$  is not an RMS so it cannot be related to the source size directly. However, it was clear from previously published analyses (see Refs. [10,27–32]) that the Lévy-scale  $R$  exhibits a similar trend as its Gaussian counterpart, namely, it decreases with  $m_T$ . In the case of a Gaussian source, hydrodynamic models predict a linear scaling for its inverse square [33–35]:

$$\frac{1}{R^2} = A \cdot m_T + B. \tag{19}$$

As we see it on Figure 7, the linear scaling holds for the Lévy source as well, requiring the need for further theoretical investigations.

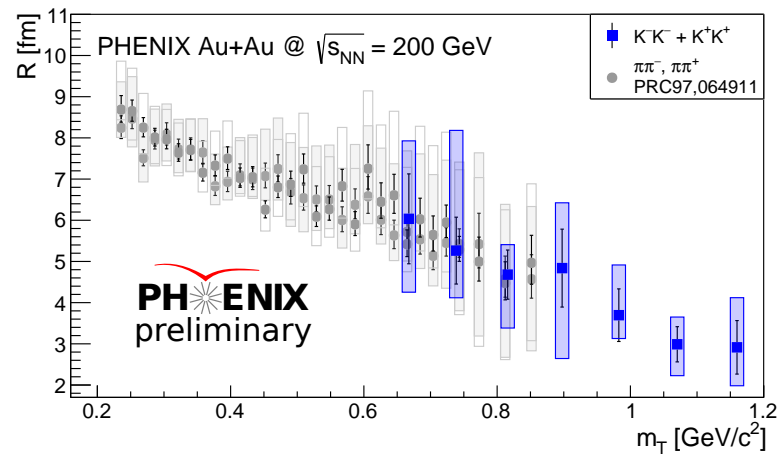


**Figure 6.** Values of the  $R$  parameter in the case of pions and kaons. Boxes indicate the systematic uncertainties, while error bars are used to represent the statistical ones.

It is worthwhile to note that there is a significant amount of point-by-point fluctuation in the systematic uncertainties. Furthermore, the non-fluctuating part of the systematic uncertainty of the pion and kaon data points is also partly correlated.

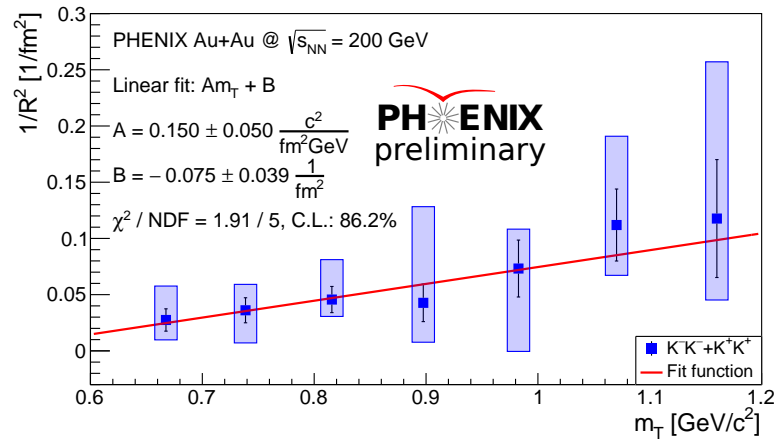


**Figure 7.** The transverse mass dependence of the  $1/R^2$  points. It is worthwhile to note that due to the large uncertainties, one could fit these data points with different powers of  $m_T$  as well. A line is fitted to the data points, and the fitted parameters are shown in the legend. Boxes indicate the systematic uncertainties, while error bars are used to represent the statistical ones.

In Ref. [10], a new empirical scaling variable was found:

$$\hat{R} = \frac{R}{\lambda(1 + \alpha)}. \quad (20)$$

The motivation behind this parameter was the fact that the  $\alpha$ ,  $R$ , and  $\lambda$  parameters are strongly correlated, and it is possible to obtain good fits with multiple sets of co-varied parameters. The discovery of  $\hat{R}$  was made without any theoretical motivation, and in Ref. [10] it was observed that  $\frac{1}{\hat{R}}$  scales linearly with  $m_T$ . In Figure 8, we can see the same linear behavior for kaons as well.

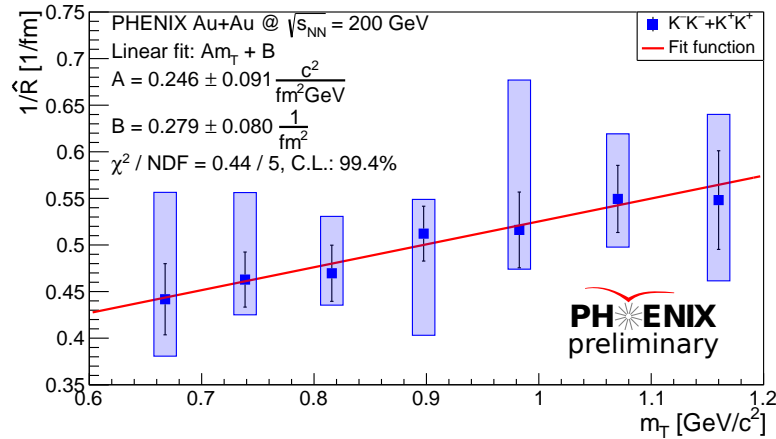


**Figure 8.** The transverse mass dependence of the  $1/\hat{R}$  points. It is worthwhile to note that due to the large uncertainties, one could fit these data points with different powers of  $m_T$  as well. A line is fitted to the data points, and the fitted parameters are shown in the legend. Boxes indicate the systematic uncertainties, while error bars are used to represent the statistical ones.

## 6. Conclusions

In this paper, we discussed two-kaon Bose–Einstein correlation functions in Au+Au collisions at  $\sqrt{s_{NN}} = 200$  GeV, from the PHENIX experiment. We assumed that the source has a Lévy shape. The Lévy parameters were investigated as functions of  $m_T$  and compared to the pion results. In the case of the Lévy stability index  $\alpha$ , the large uncertainties prevent us from drawing any strong conclusions. The prediction that was based on anomalous diffusion that  $\alpha_{Lévy}^\pi > \alpha_{Lévy}^K$  does not seem to be strongly supported. To clarify this question, further measurements and investigations might be necessary. Considering the intercept

parameter  $\lambda$ , kaons and pions have matching values at around  $m_T = 0.7 \text{ GeV}/c^2$ , and a slight decreasing trend is visible for kaons, possibly due to the worsening of the PID efficiency. The Lévy-scale  $R$  exhibits a similar trend as its Gaussian counterpart; it decreases with  $m_T$ , and its inverse square is linear in  $m_T$ , although this was predicted only for the Gaussian width. A new empirical scaling variable,  $\hat{R}$ , was found, and it was observed that  $\frac{1}{\hat{R}}$  scales linearly with  $m_T$ .

**Funding:** This research was supported by the NKFIH OTKA K-138136 grant.

**Data Availability Statement:** The data presented in this study are available on request from the corresponding author. The data are not publicly available.

**Acknowledgments:** The author would like to thank the PHENIX Collaboration.

**Conflicts of Interest:** The author declares no conflict of interest.

### Abbreviations

The following abbreviations are used in this manuscript:

HBT	R. Hanbury Brown and R. Q. Twiss
GGLP	G. Goldhaber, S. Goldhaber, W-Y. Lee, and A. Pais
RHIC	Relativistic heavy ion collider
LCMS	Longitudinal co-moving system
PCMS	Pair co-moving system
Au+Au	Gold-gold
RMS	Root mean square

### Note

<sup>1</sup> This variable can be expressed in the PCMS system, which is the pair rest frame:  $q_{\text{inv}} = |\mathbf{q}_{\text{PCMS}}|$ .

### References

1. Hanbury Brown, R.; Twiss, R.Q. A Test of a new type of stellar interferometer on Sirius. *Nature* **1956**, *178*, 1046–1048. [[CrossRef](#)]
2. Glauber, R.J. Photon Correlations. *Phys. Rev. Lett.* **1963**, *10*, 84–86. [[CrossRef](#)]
3. Glauber, R.J. Nobel Lecture: One hundred years of light quanta. *Rev. Mod. Phys.* **2006**, *78*, 1267–1278. [[CrossRef](#)]
4. Glauber, R.J. Quantum Optics and Heavy Ion Physics. *Nucl. Phys. A* **2006**, *774*, 3–13. [[CrossRef](#)]
5. Goldhaber, G.; Goldhaber, S.; Lee, W.; Pais, A. Influence of Bose-Einstein Statistics on the Antiproton-Proton Annihilation Process. *Phys. Rev.* **1960**, *120*, 300–312. [[CrossRef](#)]
6. Kopylov, G.I. Like particle correlations as a tool to study the multiple production mechanism. *Phys. Lett. B* **1974**, *50*, 472–474. [[CrossRef](#)]
7. Podgoretsky, M.I. Interference correlations of identical pions. *Sov. J. Part. Nucl.* **1989**, *20*, 266–282.
8. Csörgő, T.; Hegyi, S.; Zajc, W.A. Bose-Einstein correlations for Levy stable source distributions. *Eur. Phys. J.* **2004**, *C36*, 67–78. [[CrossRef](#)]
9. Metzler, R.; Barkai, E.; Klafter, J. Anomalous Diffusion and Relaxation Close to Thermal Equilibrium: A Fractional Fokker-Planck Equation Approach. *Phys. Rev. Lett.* **1999**, *82*, 3563–3567. [[CrossRef](#)]
10. Adare, A. et al. [PHENIX Collaboration]. Lévy-stable two-pion Bose-Einstein correlations in  $\sqrt{s_{NN}} = 200 \text{ GeV}$  Au+Au collisions. *Phys. Rev. C* **2018**, *97*, 064911. [[CrossRef](#)]
11. Yano, F.B.; Koonin, S.E. Determining Pion Source Parameters in Relativistic Heavy Ion Collisions. *Phys. Lett.* **1978**, *78B*, 556–559. [[CrossRef](#)]
12. Csörgő, T. Particle interferometry from 40-MeV to 40-TeV. *Acta Phys. Hung. A* **2002**, *15*, 1–80. [[CrossRef](#)]
13. Wiedemann, U.A.; Heinz, U.W. Particle interferometry for relativistic heavy ion collisions. *Phys. Rep.* **1999**, *319*, 145–230. [[CrossRef](#)]
14. Adler, S.S. et al. [PHENIX Collaboration]. Bose-Einstein Correlations of Charged Pion Pairs in Au+Au Collisions at  $\sqrt{s_{NN}} = 200 \text{ GeV}$ . *Phys. Rev. Lett.* **2004**, *93*, 152302. [[CrossRef](#)] [[PubMed](#)]
15. Lednicky, R.; Podgoretsky, M.I. The Interference of Identical Particles Emitted by Sources of Different Sizes. *Sov. J. Nucl. Phys.* **1979**, *30*, 432.
16. Csörgő, T.; Lörstad, B.; Zimányi, J. Bose-Einstein correlations for systems with large halo. *Z. Phys.* **1996**, *C71*, 491–497. [[CrossRef](#)]
17. Sinyukov, Y.; Lednicky, R.; Akkelin, S.V.; Pluta, J.; Erazmus, B. Coulomb corrections for interferometry analysis of expanding hadron systems. *Phys. Lett.* **1998**, *B432*, 248–257. [[CrossRef](#)]
18. Bowler, M.G. Coulomb corrections to Bose-Einstein corrections have greatly exaggerated. *Phys. Lett. B* **1991**, *270*, 69–74. [[CrossRef](#)]

19. Csanád, M.; Csörgő, T.; Nagy, M. Anomalous diffusion of pions at RHIC. *Braz. J. Phys.* **2007**, *37*, 1002–1013. [[CrossRef](#)]
20. Csanád, M.; Lökös, S.; Nagy, M. Expanded empirical formula for Coulomb final state interaction in the presence of Lévy sources. *Phys. Part. Nucl.* **2020**, *51*, 238–242. [[CrossRef](#)]
21. Csanád, M.; Lökös, S.; Nagy, M. Coulomb final state interaction in heavy ion collisions for Lévy sources. *Universe* **2019**, *5*, 133. [[CrossRef](#)]
22. Barlow, R. Systematic errors: Facts and fictions. In Proceedings of the Conference on Advanced Statistical Techniques in Particle Physics, Durham, UK, 18–22 March 2002; Volume 7, pp. 134–144.
23. Lednicky, R.; Progulova, T. Influence of resonances on Bose-Einstein correlations of identical pions. *Z. Phys. C Part. Fields* **1992**, *55*, 295–305. [[CrossRef](#)]
24. Acharya, S. et al. [ALICE Collaboration]. Kaon femtoscopy in Pb-Pb collisions at  $\sqrt{s_{NN}} = 2.76$  TeV. *Phys. Rev. C* **2017**, *96*, 064613. [[CrossRef](#)]
25. Csanád, M.; Csörgő, T. Kaon HBT radii from perfect fluid dynamics using the Buda-Lund model. *Acta Phys. Polon. Suppl.* **2008**, *1*, 521–524.
26. Csörgő, T.; Hegyi, S. Model independent shape analysis of correlations in one-dimension, two-dimensions or three-dimensions. *Phys. Lett.* **2000**, *B489*, 15–23. [[CrossRef](#)]
27. Lökös, S. Lévy-stable two-pion Bose-Einstein correlation functions measured with PHENIX in  $\sqrt{s_{NN}} = 200$  GeV Au+Au collisions. *Acta Phys. Pol. B Proc. Suppl.* **2019**, *12*, 193. [[CrossRef](#)]
28. Lökös, S. Centrality dependent Lévy-stable two-pion Bose-Einstein correlations in  $\sqrt{s_{NN}} = 200$  GeV Au+Au collisions at the PHENIX experiment. *Universe* **2018**, *4*, 31. [[CrossRef](#)]
29. Kurgyis, B.; Kincses, D.; Nagy, M.; Csanád, M. Coulomb Corrections for Bose-Einstein Correlations from One- and Three-Dimensional Lévy-Type Source Functions. *Universe* **2023**, *9*, 328. [[CrossRef](#)]
30. Kincses, D.; Nagy, M.I.; Csanád, M. Coulomb and strong interactions in the final state of Hanbury-Brown–Twiss correlations for Lévy-type source functions. *Phys. Rev. C* **2020**, *102*, 064912. [[CrossRef](#)]
31. Kincses, D. Lévy analysis of HBT correlation functions in  $\sqrt{s_{NN}} = 62$  GeV and 39 GeV Au+Au collisions at PHENIX. *Universe* **2018**, *4*, 11. [[CrossRef](#)]
32. Kurgyis, B. Three dimensional Lévy HBT results from PHENIX. *Acta Phys. Pol. B Proc. Suppl.* **2019**, *12*, 477–482. [[CrossRef](#)]
33. Chapman, S.; Scotto, P.; Heinz, U. New Cross Term in the Two-Particle Hanbury-Brown–Twiss Correlation Function in Ultrarelativistic Heavy-Ion Collisions. *Phys. Rev. Lett.* **1995**, *74*, 4400–4403. [[CrossRef](#)] [[PubMed](#)]
34. Makhlin, A.N.; Sinyukov, Y.M. Hydrodynamics of Hadron Matter Under Pion Interferometric Microscope. *Z. Phys. C* **1988**, *39*, 69. [[CrossRef](#)]
35. Csörgő, T.; Lörstad, B. Bose-Einstein correlations for three-dimensionally expanding, cylindrically symmetric, finite systems. *Phys. Rev. C* **1996**, *54*, 1390–1403. [[CrossRef](#)] [[PubMed](#)]

**Disclaimer/Publisher’s Note:** The statements, opinions and data contained in all publications are solely those of the individual author(s) and contributor(s) and not of MDPI and/or the editor(s). MDPI and/or the editor(s) disclaim responsibility for any injury to people or property resulting from any ideas, methods, instructions or products referred to in the content.